Sparse Metasurfaces for Scattering Cross Section Reduction of Arbitrarily Shaped Metallic Bodies

François Villamizar, Cédric Martel, Fabrice Boust, Shah Nawaz Burokur

Sparse metasurfaces for scattering cross section reduction of arbitrarily-shaped metallic bodies

François Villamizar[§], Cédric Martel[§,], Fabrice Boust[‡], and Shah Nawaz Burokur[‡,]**

[§]ONERA / DEMR, Université de Toulouse, F-31055 Toulouse, France

[‡]DEMR, ONERA, Université Paris-Saclay, F-91123 Palaiseau, France

[‡]LEME, UPL, Univ Paris Nanterre, F92410 Ville d'Avray, France

*Corresponding authors

KEYWORDS: scattering cross section, cloaking, Green's function, conformal, sparse metasurfaces

ABSTRACT: Reducing the scattering cross section (SCS) of metallic objects plays a key role in stealth technology. In this work, sparse metasurfaces are designed through numerical calculations of Green's functions and are proposed to reduce the electromagnetic scattering of metallic cylinders. The metasurfaces are composed of relatively sparse meta-atoms limited only by the impedance density without considering any resonance factor. The diameter of the metallic cylinders is of the order of one wavelength around the operating frequency of 5 GHz. By optimizing the load impedance distribution of the sparse metasurfaces coating the cylinders, the scattering cross section of the cylinders can be considerably reduced. To experimentally demonstrate the concept, several prototypes are fabricated and tested in a microwave anechoic

chamber. The experimental measurements are in good agreement with the numerical simulations and verify the consistent performance of the metasurfaces in SCS reduction.

INTRODUCTION

In the military domain, substantive research studies are carried out towards reducing the SCS, particularly the monostatic SCS commonly known as the radar cross section (RCS), of carriers to avoid detection from radar systems. Historically, electromagnetic absorbers, such as the Salisbury screen[1] and later, Jaumann layers,[2] were introduced after the second World War in order to reduce the scattered fields of objects. These absorbers are composed of homogenous resistive sheets, with different resistivity, separated by a distance of quarter-wavelength to absorb power from the incident wave. Hand in hand with the deployment of modern multistatic radar systems, reducing the backscattering of targets illuminated by several emitters has become mandatory in stealth applications. In the field of antennas and communication systems, avoiding the interaction between neighboring antennas or between antennas and their supporting structures, is essential to improve communication links.[3,4] More recent developments of absorbing structures make use of circuit analog absorbers where resistive sheets are replaced by frequency selective surfaces (FSSs). In particular, high impedance surfaces are exploited to minimize reflection over a broad frequency range.[5,6]

In the meantime, metasurfaces with reduced profile have proven to be a powerful tool in wavefront manipulation.[7,8] Studies related to planar metasurfaces have further been extended to curved and arbitrarily-shaped metasurfaces.[9–11] Conformal metasurfaces enable meeting the aerodynamic requirements of communication platforms and vehicles. They are generally designed using geometrical optics approach,[9,11] where a proper spatial distribution of the local reflection or transmission coefficient must be established along the metasurface. However, such approach presents strong limitations in terms of efficiency.[12] A more accurate procedure, which remains quite challenging, consists in establishing a relationship between a given coordinate

system and another one that conforms the geometry of the curved interface.[10] As such, planar and conformal metasurfaces, composed of resonant elements separated from a ground plane by a lossy dielectric material, have been successfully applied for the design of absorbing structures[13-18] and invisibility coatings.[19-22]

While the most generally applied generalized laws of reflection and refraction tend to suffer from low efficiency,[12,23] metagratings with sparse arrangement of judiciously engineered scatterers have been proposed to boost the wavefront manipulation efficiency[24-27] and have been further exploited to design electromagnetic absorbers by suppressing the specular reflection.[28-29] Sparse metasurfaces,[30–31] evolving from metagratings, are capable of creating arbitrary radiation patterns for arbitrary external illuminations and have demonstrated high efficiency in tailoring wavefronts. They are non-periodic structures composed of a finite set of loaded wires with an inter-element distance of the order of the operating wavelength λ_0. Sparse metasurfaces are strongly nonlocal and cannot be described using either the surface impedance density or using local reflection/transmission coefficients. While Green's functions for simple geometries in free space environment are well known, it is generally not the case for more complex geometries and environments, where the Green's function cannot be analytically calculated. As such, sparse metasurfaces are designed by numerical calculation of the Green's function and do not use any complex coordinate system matched to a particular geometry, thereby allowing arbitrarily shapes to be considered.

In this work, we propose an alternative design concept of passive conformal sparse metasurface absorbers, capable of reducing the scattering cross section (SCS) of metallic objects having dimensions of the order of one wavelength. The general design methodology is described and numerical simulations that are backed up by experimental measurements carried out on fabricated samples, validate the proposed approach. Such a design concept fully based upon calculation of Green's function is easy to implement and opens the door to future development

of thin conformal and smart skins for diverse applications, including electromagnetic compatibility and interference, decoupling in antenna systems, stealth and camouflaging.

DESIGN PROCEDURE OF SPARSE METASURFACES

Let us consider a sparse metasurface coating a metallic cylinder and illuminated by an incident plane wave E_0 polarized along the z-axis, which propagates towards decreasing x-values, as depicted in Figure 1a,b. The metasurface is composed of N equally distributed loaded wires on a flexible substrate. Macroscopically, the wires are modeled as thin cylinders of effective radius r_{eff} ($<< \lambda$) oriented along the translation invariant direction (z-axis) and are characterized by an impedance density. Electric fields from external sources excite polarization currents I_q along the wires, which in turn scatter an electric field. No condition is required for the external sources; they can be of any type. According to the impedance densities imposed to the set of wires, the field radiated in the far field region can be controlled and tailored to favor the scattering in desired directions using:

$$E_z(r,\varphi) = E_z^{ext}(r,\varphi) + \sum_{q=1}^{N} G_{zz}\left(r,\varphi;\mathbf{r}_q\right) I_q \qquad (1)$$

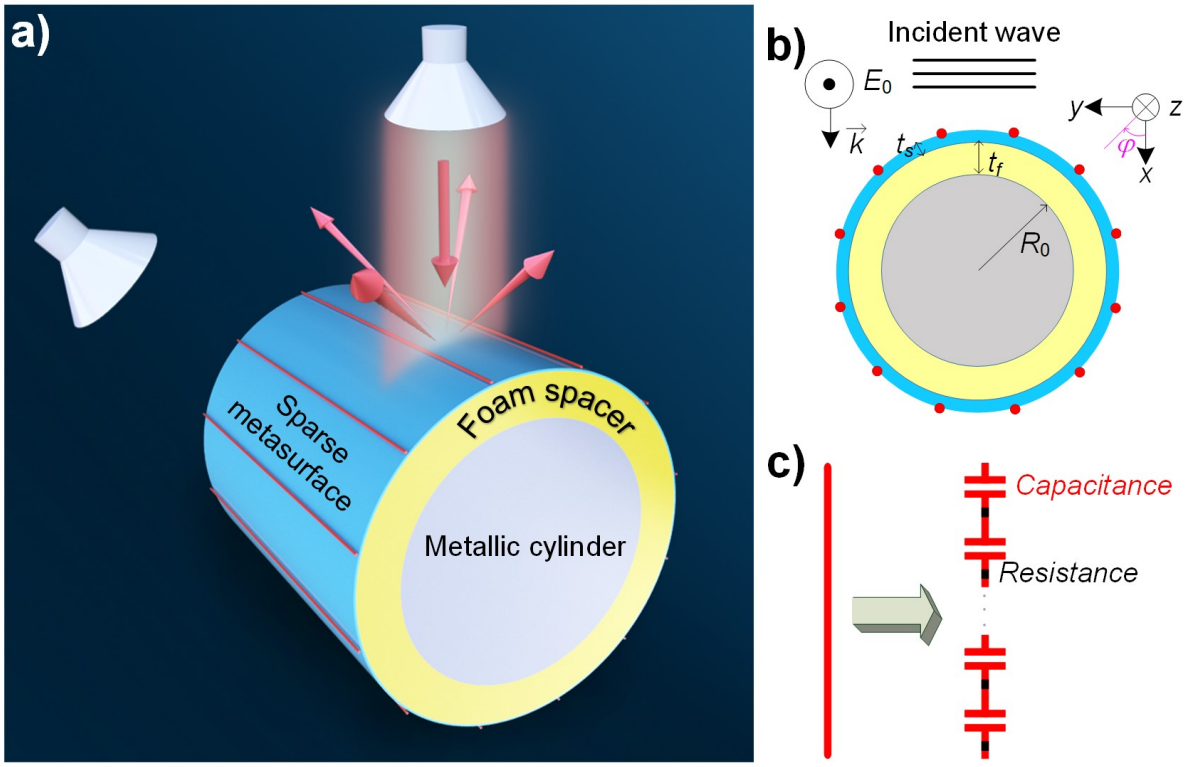

Figure 1. (a) Operating principle of the scattering cross section reduction using a sparse metasurface. (b) Schematic view of a metallic cylinder coated by a flexible sparse metasurface and illuminated by an external electric field E_0. The metallic cylinder having radius $R_0 = 30$ mm is coated with the conformal sparse metasurface, with a foam spacer of thickness $t_f = 9.5$ mm and relative permittivity $\varepsilon_f = 1.15$ in between. The metasurface is composed of 12 loaded wires equally distributed on a flexible F4BM220 substrate having a thickness $t_s = 0.5$ mm and relative permittivity $\varepsilon_s = 2.2$. (c) For the experimental validation, the loaded wires are implemented by microstrip structures loaded with resistors.

Here, $E_z(r,\varphi)$ is the total scattered field, which is a superposition of $E_z^{ext}(r,\varphi)$, the field scattered by solely the external sources in absence of the wires, and the waves $G_{zz}(r,\varphi;\mathbf{r}_q)\, I_q$ scattered by the loaded wires. $G_{zz}(r,\varphi;\mathbf{r}_q)$ is the Green's function of the q^{th} wire, positioned at $\mathbf{r}_q$ in the polar coordinates (r,φ) and I_q is the polarization line current excited in the q^{th} wire. The polar angle φ is measured from the direction of the x-axis, as illustrated in Figure 1.

In such sparse metasurfaces, Ohm's law links the field radiated by the wires, the currents and the load impedance densities, as:

$$Z_q I_q = E_z^{ext}(\mathbf{r}_q) - \sum_{p=1}^{N} Z_{qp}^{(m)} I_p, \qquad (2)$$

where Z_q is the q^{th} wire's load impedance density and $Z_{qp}^{(m)} = -G_{zz}(\mathbf{r}_q, \mathbf{r}_p)$ is the mutual-impedance density linking the electric field created by the p^{th} wire at the position of the q^{th} wire. $Z_{qq}^{(m)}$, the self-action of the q^{th} wire and its interaction with the external environment, is calculated by:

$$Z_{qq}^{(m)} = -\frac{1}{2\pi r_{eff}} \oint G_{zz}(\mathbf{r}, \mathbf{r}_q) d\mathbf{r}, \qquad (3)$$

where the integration is done over the circumference of the thin wire with effective radius r_{eff}. By choosing the number of wires N and the load impedance densities Z_q appropriately, the scattered far field $E_z(r, \varphi)$ can be efficiently controlled.

Here, our main goal is to reduce the cylinder's backscattering in order to avoid its detection by a radar system, as illustrated in Figure 1a. By setting $E_z(r, \varphi) = 0$ and solving eq 1 analytically, the scattering can be reduced in a number of desired directions. Even the forward scattering, known as the shadow region of the object can be reduced, but this would require the use of active and lossy wires, for which the optical theorem does not apply. A classical differential evolution algorithm,[32-33] which takes the load impedance densities as candidate solutions, is used to minimize the scattering in the desired directions. Microscopically, in order to replace the infinitesimal wire model with a wire built up from physically feasible unit cells (Figure 1c), we need to restrict the real part of the load impedance density to positive values.

SCATTERING REDUCTION OF A METALLIC CYLINDER

The methodology is first applied for the design of a sparse metasurface conformed to a circular metallic cylinder having radius $R_0 = \lambda_0/2 = 30$ mm, with λ_0 being the operating wavelength, as illustrated in Figure 1b. Such radius value is a design choice regarding the targeted application

and is typically the case for metallic circular ducts supporting antennas. We are interested in reducing both the monostatic and bistatic scattering around f_0 = 5 GHz. The metallic cylinder is first coated with a foam sapcer of thickness t_f = 9.5 mm and relative permittivity ε_f = 1.15, onto which is conformed the sparse metasurface. The metasurface is composed of 12 wires equally distributed on the top face of a flexible F4BM220 substrate having a thickness t_s = 0.5 mm, relative permittivity ε_s = 2.2 and a loss tangent tan δ = 0.001.

We are first interested in reducing the monostatic SCS of the metallic circular cylinder for an incident plane wave varying from φ = 0° to 360°. In such monostatic configuration, the observer is located at the same position as the incident wave. In this case, the commonly known radar cross section term can be used, which corresponds to the backscattering configuration. Since the cylinder has a circular base, a rotational symmetry around the *z*-axis is present. Therefore, for the metasurface, the same load-impedance density is imposed on the 12 wires distributed equally on the substrate. In order to reduce the backward scattering in such a scenario, a fitness function that minimizes the back-scattered field is used in the minimization algorithm.

We further target the scattering reduction in various directions in a bistatic configuration. The structure is illuminated by a plane wave at incidence φ = 0° and scattering is measured from φ = 0° to 180°. Hence, another metasurface also composed of 12 wires, is designed. However, owing to the symmetry of the body, only six models of wires are necessary. The fitness function used in the minimization algorithm in order to find the correct impedance densities for the bistatic SCS reduction:

$$f_{goal}(Z_1, Z_2, \dots Z_N) = \sum_i^N |E_z(\varphi_i)| \quad (4)$$

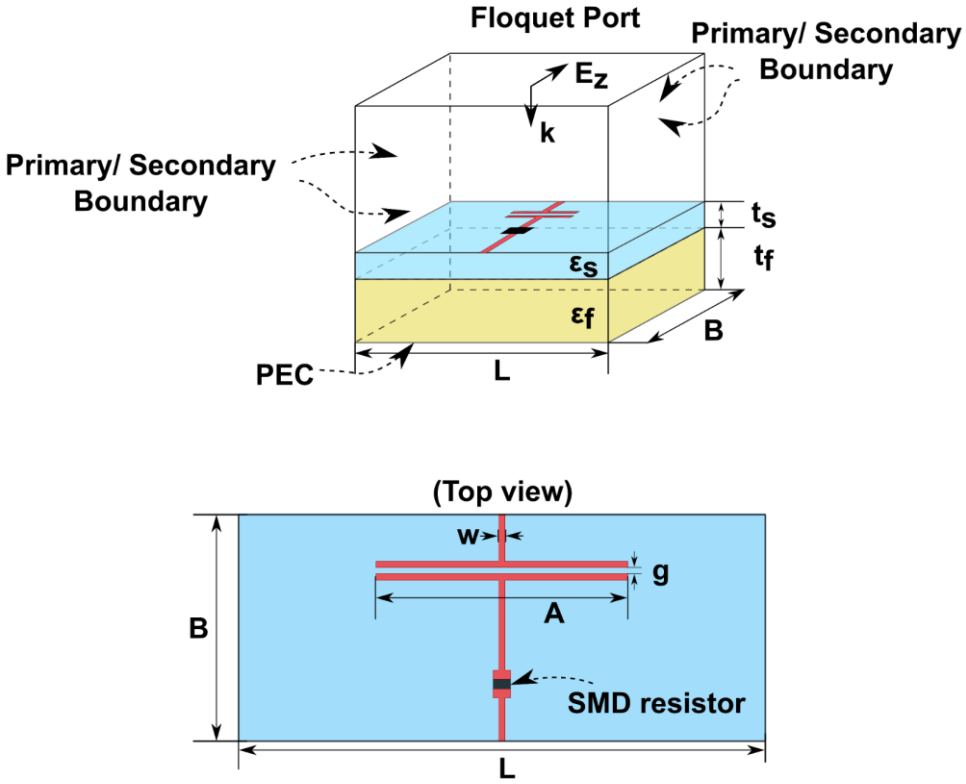

Figure 2. Schematic of the employed unit cell, comprised of a F4BM 220 substrate with a printed wire, a foam spacer and a ground plane (t_s = 0.5 mm, ε_s = 2.2, t_f = 9.5 mm, ε_f = 1.15). The wire is composed of a 0402 SMD resistor for the lossy part and a printed capacitor for the imaginary part. The geometrical parameters are L = 21 mm, B = 9 mm, w = 0.25 mm, g = 0.25 mm and A is a variable (see Table 1).

The required load impedance density of the wires is then calculated using the differential evolution algorithm and implemented using realistic wires built up from meta-atoms. The local periodic approximation (LPA), detailed in the Methods section, is used to retrieve the respective impedance density from the reflection coefficient characterized from the meta-atom.[34] For a practical implementation, we are interested in load impedance densities that generally possess a positive real part (lossy) and an imaginary part, which can be negative (capacitive) or positive (inductive). In practice, the impedance can be obtained from printed microstrip structures for the reactive component and loaded with serial SMD resistors to materialize the passive and lossy component, as depicted in Figure 1c. In the simulations, the SMD resistors are modeled

as a simple resistive sheet, while Vishay CH0402 resistors are used in the fabricated samples. A schematic view of the resistor loaded unit cell in its simulation setup is shown in Figure 2. The retrieved load-impedance density Z_q and the parameters of the unit cell are reported in Table I. The given impedance densities are normalized by the multiplication factor λ_0/η, where η is the characteristic impedance in free space.

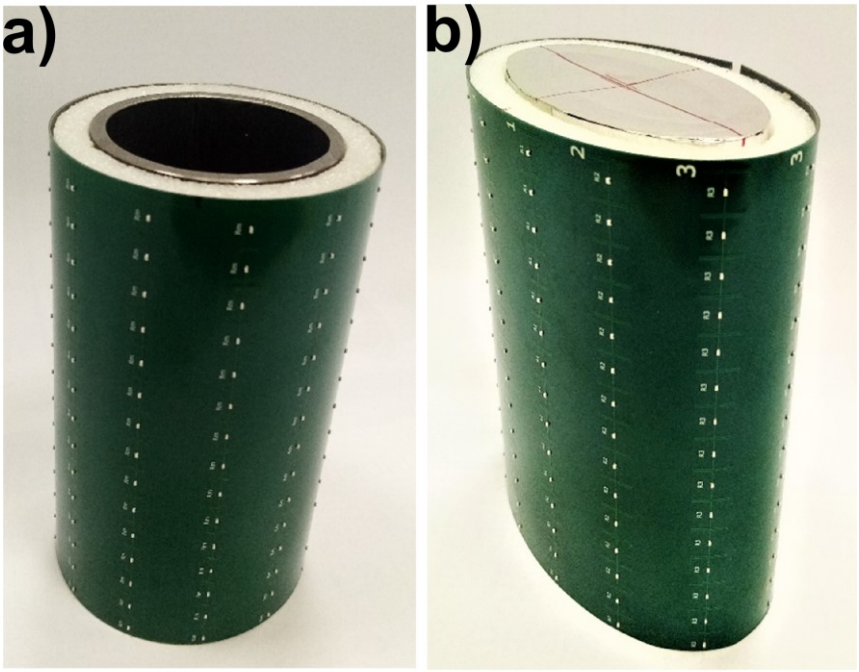

Figure 3. Photograph of the proof-of-concept prototypes. (a) Metasurface-coated metallic circular cylinder. (b) Metasurface-coated metallic elliptical cylinder.

Table 1. Characteristics of the Meta-Atoms for SCS Reduction in Different Scenarios

Scenario		**Element Number**					
		1	**2**	**3**	**4**	**5**	**6**
monostatic (circular)	*Zq* (η/λ)	2.3-*j*5.9	NA	NA	NA	NA	NA
	Resistor Value (Ω)	100	NA	NA	NA	NA	NA
	A (mm)	4.23	NA	NA	NA	NA	NA
bistatic (circular)	*Zq* (η/λ)	2.9-*j*5.4	2.1-*j*6.0	1.6-*j*6.8	1.3-*j*8.2	29-*j*52.8	-*j*1.2
	Resistor Value (Ω)	150	100	50	50	150	NA
	A (mm)	4.64	4.15	3.59	2.86	1.49 (2 capacitors)	10
monostatic (elliptical)	*Zq* (η/λ)	2.39-*j*3.35	1.86-*j*2.9	2.33-*j*2.97	NA	NA	NA
	Resistor Value (Ω)	150	100	150	NA	NA	NA
	A (mm)	7.86	9	8.91	NA	NA	NA
cloaking (circular)	*Zq* (η/λ)	2.5-*j*5.5	2.2-*j*6.3	0.88-*j*7.3	-0.88-*j*7.3	-2.2-*j*6.3	-2.5-*j*5.5

RESULTS AND DISCUSSION

Numerical simulations are performed using the commercially available full wave electromagnetic simulator HFSS. A metasurface-coated cylinder having a height of 9 mm, equivalent to the height *B* of one meta-atom (Figure 2), is considered along the *z*-axis. Periodic boundary conditions are applied in the *xoy* planes at the top and bottom to consider an infinitely high structure. The structure is surrounded by a cylindrical vacuum, upon which radiation boundary conditions are assigned on the curved face, which enables far-field simulations. The cylinder is then illuminated by a plane wave having the electric field oriented along the *z*-axis and incident with an angle φ, as presented in Figure 1b. The scattering width σ_{2D} in unit meters (m) is then obtained using the procedure described in the Methods section. In the experiments, a cylinder having a height of 135 mm is considered and the metasurface coat is composed of 15 meta-atoms along the *z*-axis. A photograph of the fabricated proof-of-concept prototype is shown in Figure 3a for the circular cylinder scenario and in Figure 3b for the elliptical cylinder scenario. The measurements performed in an anechoic chamber, as detailed in the Methods section, correspond to a scattering cross section σ_{3D} in unit square meters (m^2). Consequently, in order to compare the simulation results with experimental ones, as depicted in Figure 4, σ_{2D} and σ_{3D} are linked together using eq 10. The metasurface composed of 12 wires with similar load-impedance density equally distributed on the substrate, as illustrated in Figure 4a, is exploited for the monostatic SCS measurement. As shown in Figure 4b, the measurements performed in the monostatic configuration demonstrate backscattering reduction capacities of the metasurface coating of at least 10 dB in the frequency band spanning from 4.3 GHz to 4.9 GHz. To better highlight the reduction level, comparison of the backscattering of the bare and metasurface-coated cylinders are presented at 4.8 GHz in Figure 4c. The sparse metasurface coating achieves a backscattering reduction of at least 14.75 dB all around the circular cylinder.

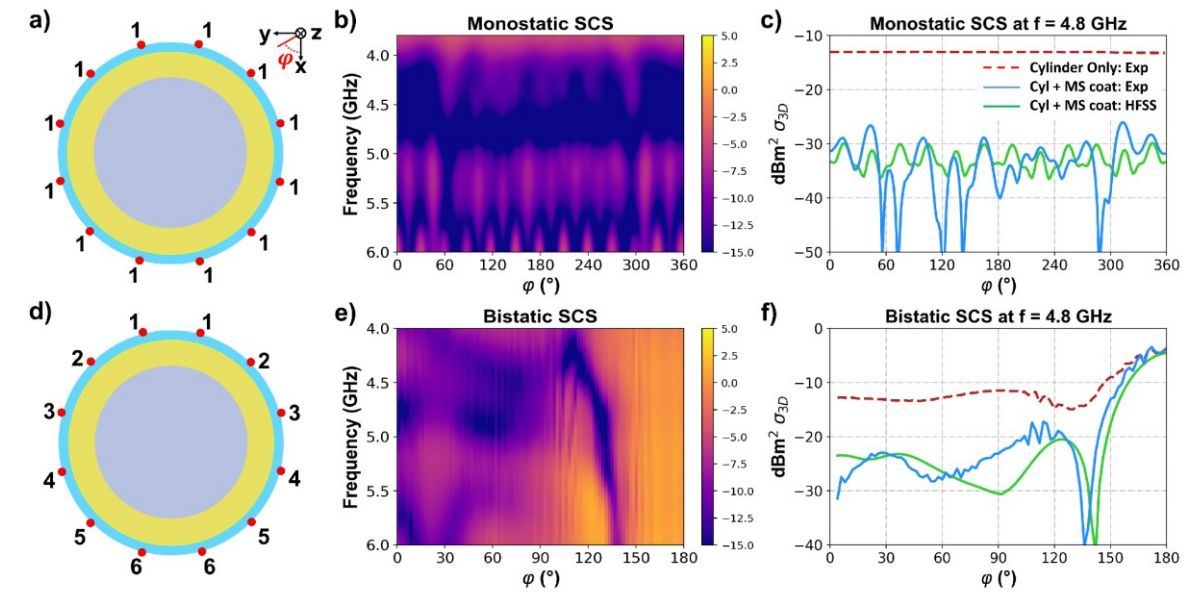

Figure 4. SCS reduction of a circular cylinder under plane wave illumination (Top row: monostatic configuration and bottom row: bistatic configuration). (a), (d) Schematic of the structure (metasurface-coated cylinder). (b), (e) SCS reduction level versus frequency. (c), (f) SCS level of coated and uncoated cylinders at 4.8 GHz.

Similarly, bistatic scattering cross section measurements is carried out on a prototype where the metasurface is composed of also 12 wires to reduce scattering in various directions. However, due to the symmetry of the cylinder, only six models of wires are required, as illustrated in Figure 4d. For φ running from 4° to 180°, a total SCS reduction of at least 9.5 dB in the 4.5 GHz - 5 GHz frequency band is observed, as depicted in Figure 4e. Above 5 GHz, the SCS increases for φ lying in the range 95° - 130°. At 4.8 GHz, the total scattering cross section $\sigma_{3D_{tot}}$, as defined in eq 11, of the non-coated (bare) cylinder is measured to be -11.48 dBm^2. With a metasurface coating, the experimental total scattering cross section $\sigma_{3D_{tot}}$ is -21.14 dBm^2, which is equivalent to a reduction of 9.66 dB. Significant backscattering reduction of σ_{3D} (φ_{back}) of 18.7 dB is also observed in Figure 4f. It is worthwhile noting that the simulation results obtained from infinitely long structures using Ansys HFSS show a good qualitative

agreement with the experimental measurements of structures of finite height for both the monostatic and bistatic SCS cases.

In order to extend the concept of backscattering reduction to a more complex shape, we consider an elliptical metallic cylinder of minor axis $2a = 45$ mm and major axis $2b = 90$ mm, as depicted in Figure 5a. 12 wires are distributed around the substrate, so that the distance between two adjacent wires arranged around the perimeter of the ellipse is equal. Due to the absence of rotational symmetry, three different load-impedance densities are required to reduce the monostatic SCS. For the experimental validation, a fully dielectric elliptical cylinder is fabricated using 3D-printing technology and carefully coated with a thin layer of conductive aluminum tape to mimic a metallic one (Figure 3b). The results are presented in Figure 5b, where a slightly lower reduction level is observed in measurements compared to simulations. At 4.7 GHz, the SCS is reduced by 11.67 dB at $\varphi = 206°$, while a reduction of only 2.56 dB at $\varphi = 300°$ is achieved with the sparse metasurface. Even though the sparse metasurface conformed to an elliptic cylinder is less efficient for certain incidence angles, the results prove that the methodology can be applied to objects having complex shapes, without increased difficulty.

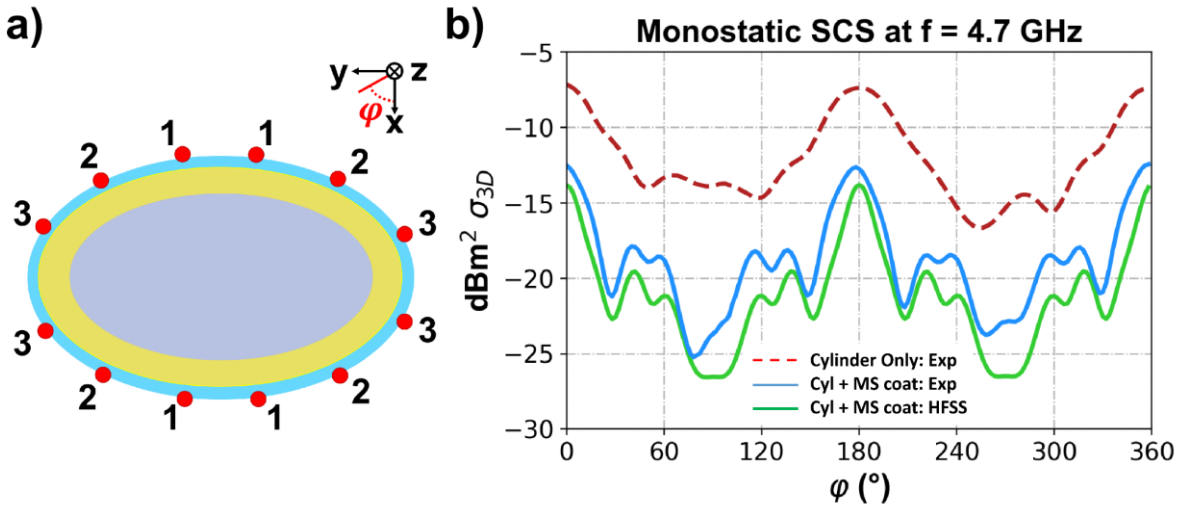

Figure 5. (a) Schematic illustration of the SCS reduction of the elliptical cylinder. (b) Monostatic SCS level of the coated and uncoated elliptical cylinders at 4.7 GHz.

As it can be observed from the performances obtained from both the cylindrical and elliptical cylinders, there are slight discrepancies between simulation and experimental results that are mainly attributed to the lumped resistors. In simulations, the SMD resistor is modelled as a simple resistive sheet that does not take into account the pad welding and parasitic effects encountered in the experiments. Nevertheless, the metasurfaces did not show significant performance drops when replacing the exact resistor values calculated by the minimization algorithm with the closest one proposed by the Vishay resistor family.

Finally, the proposed design methodology is exploited to cloak the metallic cylinder. However, instead of using a minimization algorithm, the required impedance density of the 6 models of wires on the metasurface are determined analytically (Figure 6a). The calculated load impedance densities then have positive and negative real parts, which implies the use of lossy and active elements, as shown in Table 1. It is important to note that the wires noted 1, 2 and 3 show the same imaginary parts of the load impedance density as wires noted 4, 5 and 6, respectively, but with opposite real parts, suggesting that the fields absorbed in the back semi-space of the cylinder are emitted in the front semi-space. In this configuration, the total SCS $\sigma_{3D_{tot}}$ reduction is around 50 dB. Even the forward scattering is reduced, as depicted in Figure 6b and highlighted by the absence of shadow behind the object in the inset presenting the wavefronts. The result obtained from a simulation performed using ideal loaded wires indicate that cloaking of a metallic cylinder is indeed possible using the proposed approach. However, both passive and active load impedance densities are necessary, which can be quite challenging in a practical implementation.

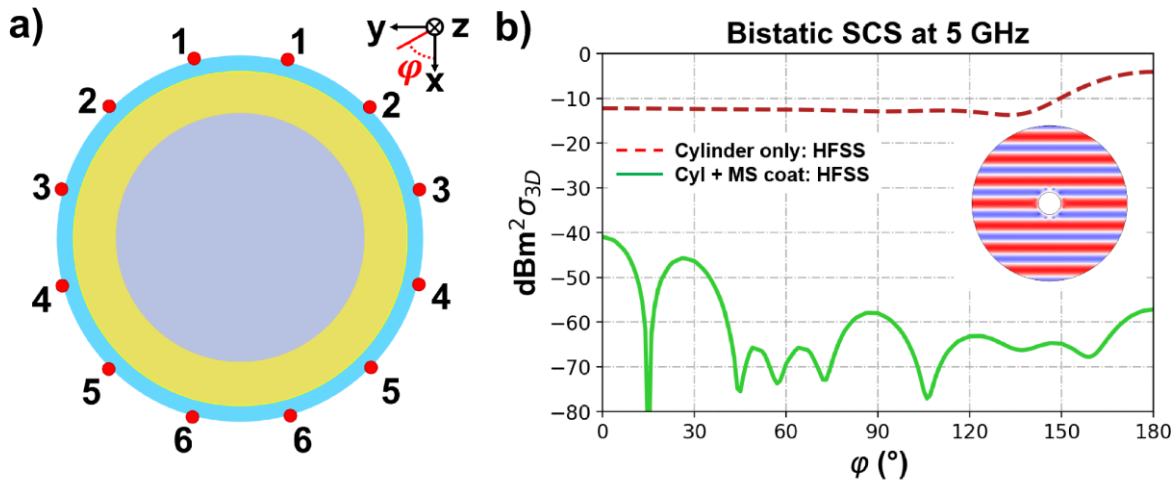

Figure 6. Simulation of the SCS level of a coated and uncoated cylinder at 5 GHz using 12 active infinitesimal wires.

CONCLUSIONS

A simulation-based design procedure using Green's functions is exploited to design conformal sparse metasurfaces capable of reducing the scattering cross section of a translation invariant metallic cylinder. A first sparse metasurface is proposed to reduce the SCS of a circular cylinder in a monostatic configuration. The backscattering of the cylinder is reduced by at least 14.75 dB at 4.8 GHz, for any angle of incidence. A second metasurface capable of reducing the bistatic SCS of that cylinder is also designed. A total SCS reduction is achieved (9.66 dB at 4.8 GHz). Furthermore, interesting results are obtained when considering an elliptical cylinder, demonstrating that the methodology can be applied to arbitrarily-shaped objects, without further difficulty. The manufacturing simplicity of these metasurfaces, only consisting of flexible PCB and standard surface mount resistors, makes them good candidates as suitable and cost-effective solution for scattering cross section reduction and absorption devices. Finally, in an attempt to realize cloaking with our proposed approach, ideal bistatic simulations have highlighted scattering reduction in all directions, including the forward scattering, when using a metasurface implementing passive as well as active wires. The proposed design methodology,

comprising numerical calculations of Green's functions and materializing load impedance via local periodic approximation, constitute an alternative means to design planar and conformal metasurfaces for various functionalities, including beamforming. Moreover, the sparse feature of the proposed metasurfaces suggests that few elements would be required when considering reconfigurability aspects. The main results of this study paves the way to the design of thin conformal and smart skins for electromagnetic compatibility and interference, decoupling in antenna systems, stealth and camouflaging.

METHODS

Numerical calculations leading to the load impedance Z_q

The metal cylinder together with the surrounding dielectric materials (in the absence of the wires) is illuminated by a plane wave. The far field, which is composed of only the diffracted field as well as the total field on the contour of the substrate (referred to as C1 here) where the wires will be placed, are recorded, as depicted in Figure 7. These fields allow calculating $E_z^{ext}(r,\varphi)$ of eq 1 and $E_z^{ext}(\mathbf{r}_q)$ of eq 2.

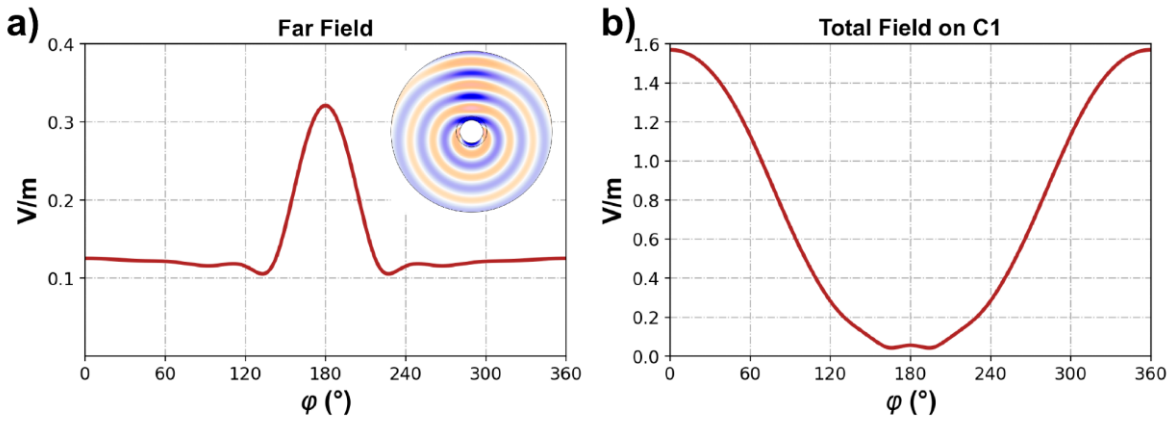

Figure 7. Recorded electric field when the metal cylinder with its surrounding dielectrics (in the absence of the wires) is illuminated by a plane wave. (a) Far field. (b) Total field on the contour C1 where the wires are supposed to be located.

One of the 12 wires is placed on the contour C1 (for example at $\varphi_q = 90°$) and the far field radiated by the wire when driven by an intensity of 1 A is calculated, as shown in Figure 8a. The wire must be very small; its radius is fixed as $r_{eff} = 0.0625$ mm. The field radiated by the wire at locations φ_p of the other 11 wires on the contour C1 is also recorded and presented in Figure 8b. For the cylinder, only one calculation is required and the fields corresponding to the other 11 wires are obtained simply by shifting by 2π/12 the field already calculated for the wire at $\varphi_q = 90°$. However, for the elliptical cylinder, three calculations are required since three models of wires are used, as depicted in Figure 5.

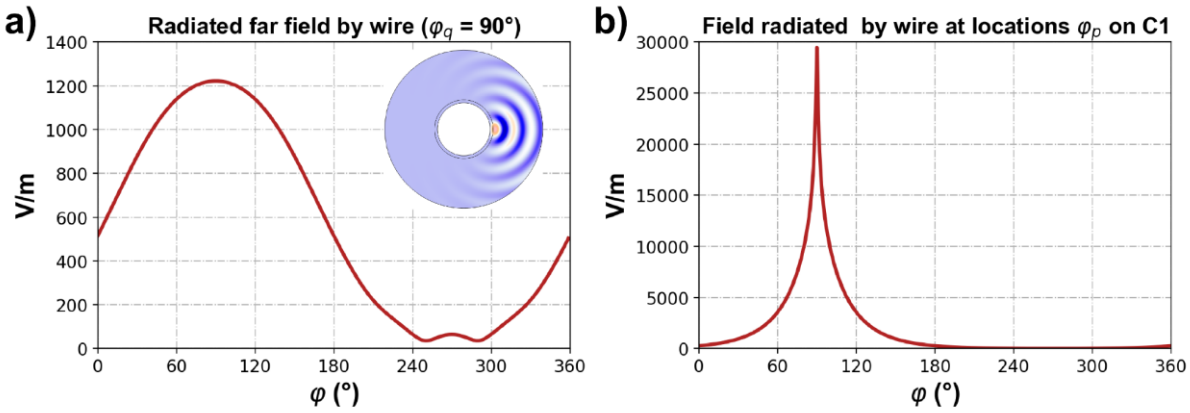

Figure 8. Recorded electric field when a wire driven by a current of 1 A is located at $\varphi_q = 90°$ on the contour C1. (a) Far field radiated by the wire. (b) Total field radiated by the wire at locations φ_p of the other 11 wires on the contour C1.

At this stage, the average field of the wire can be obtained by integrating the field at the surface of the wire and then dividing by $2\pi r_{eff}$. Since the intensity of the current in the wire is 1 A, we can then have the impedance density Z_{qq} appearing in eq 3. In our case, the numerical value is 8400+j37000 Ω/m. This value has to be compared with that of an isolated wire of similar radius, which is $\frac{k\eta}{4} H_0^2(kr_{eff}) = 9876+j32345$ Ω/m (k is the wave vector and H_0^2 is the Hankel function

of the second kind). The far field radiated by each wire at location φ_q give the terms $G_{zz}(r, \varphi; \mathbf{r}_q)$ of eq 1.

The field radiated at φ_p by the wire placed at φ_q allows calculating the terms of $Z_{qp}^{(m)}$ of eq 2. The matrix of the mutual impedance densities Z_{qp} in Figure 9 shows that as we move away from the neighboring wires, the coupling is strongly reduced.

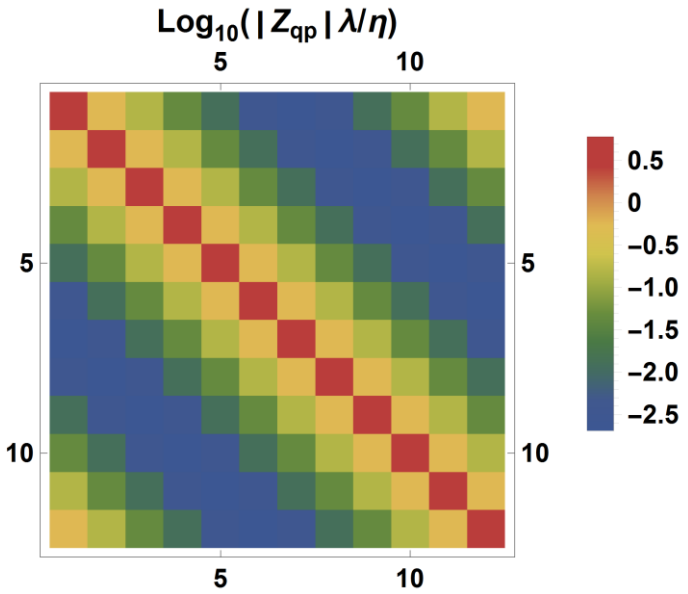

Figure 9. Matrix of the mutual impedance densities Z_{qp}.

Local periodic approximation

In the case of traditional dense metasurfaces, the LPA allows calculating the surface impedance corresponding to a given elementary cell when it is periodically arranged to form a metasurface. For metagratings, the LPA described in Ref. 34 is used to calculate the linear impedance (denoted Z_q) of a wire equivalent to a set of connected cells. The procedure is as follows:

- analytically calculate the reflection coefficient of an array of thin wires of linear impedance Z_q and period L

- using a full wave method, calculate the reflection coefficient for normal plane wave illumination of the 3D elementary cell that is repeated periodically in the y direction with a period L (Figure 2).

The periodicity L must be large enough such that the interaction between two neighboring wires is correctly represented by the interaction between two wires assumed infinitely thin, while remaining less than λ to avoid appearance of diffracted orders.

When the array of thin wires is illuminated by an incident plane wave, a polarization line current of intensity I is excited in each wire:

$$I = -\frac{2L}{\eta}\frac{(S_0 - R_0 e^{2jkh})}{(1+R_0)e^{2ikh}}E_0, \quad (5)$$

where S_0 is the reflection coefficient (in the plane of the pattern) obtained from the full wave simulation of the elementary cell and R_0 is the analytically calculated Fresnel's reflection coefficient from the grounded substrate in the absence of the wires. Here, h is the total dielectric thickness ($h = t_f + t_s$). E_0 is the amplitude of the incident electric field, and k and η are, respectively, the wavenumber and the characteristic impedance in free space.

The current I is linked to the wire's impedance by Ohm's law:

$$Z_q = \frac{E_{ext}}{I} - \frac{k\eta}{4} - Z_m, \quad (6)$$

where $E_{ext} = (1 + R_0)E_0\exp(ikh)$ is the total external electrical field, which is the sum of the incident field and its specular reflection from the ground plane and $\frac{k\eta}{4}$ is the radiation resistance of the wire. Z_m is the mutual impedance density, which takes in consideration the interaction of a loaded wire with the grounded substrate and the interaction between adjacent wires, and is given as:

$$Z_m = \frac{k\eta}{2}\sum_{n=1}^{\infty} H_0^{(2)}(knL) + \frac{\eta}{2L}R_0 \quad (7)$$

It is important to note that considering Z_m allows using the calculated linear impedance Z_q in configurations where the distance between wires is different to the periodicity L used in the LPA here.

Experimental measurements

The metallic cylinder is surrounded by a foam spacer of permittivity $\varepsilon_f = 1.15$ and thickness $t_f = 9.5$ mm. The metasurfaces are composed of a 0.5 mm thick flexible F4BM220 dielectric substrate on which copper traces are patterned and SMD Vishay CH0402 resistors are soldered using pick-and-place technology. The metasurfaces, having dimensions of 135 mm × 248 mm for the circular cylinder and 135 × 276.5 mm for the elliptical cylinder, are wrapped around the foam spacer using adhesive tape.

The experimental setup is schematically illustrated in Figure 10. The sample is fixed on top of a low index material rotating platform in the middle of a calibrated anechoic chamber. Mobile emitting and receiving horn antennas are used in order to measure the SCS from 3.5 to 8 GHz with a frequency step of 10 MHz. When performing bistatic measurements, the emitting horn antenna and the rotating platform are maintained at a fixed position, while the receiving horn is moved along a circular track to record the scattered field from 4° to 180° with an angular step of 2°. When performing monostatic measurements, both horn antennas are set in a quasi-monostatic configuration and held at a fixed position, while the platform is rotated from 0° to 360° with an angular step of 2°. A reference measurement of solely the anechoic chamber without any sample is performed in order to measure the noise due to surrounding environment. The recorded reference data is then subtracted from the SCS measurements.

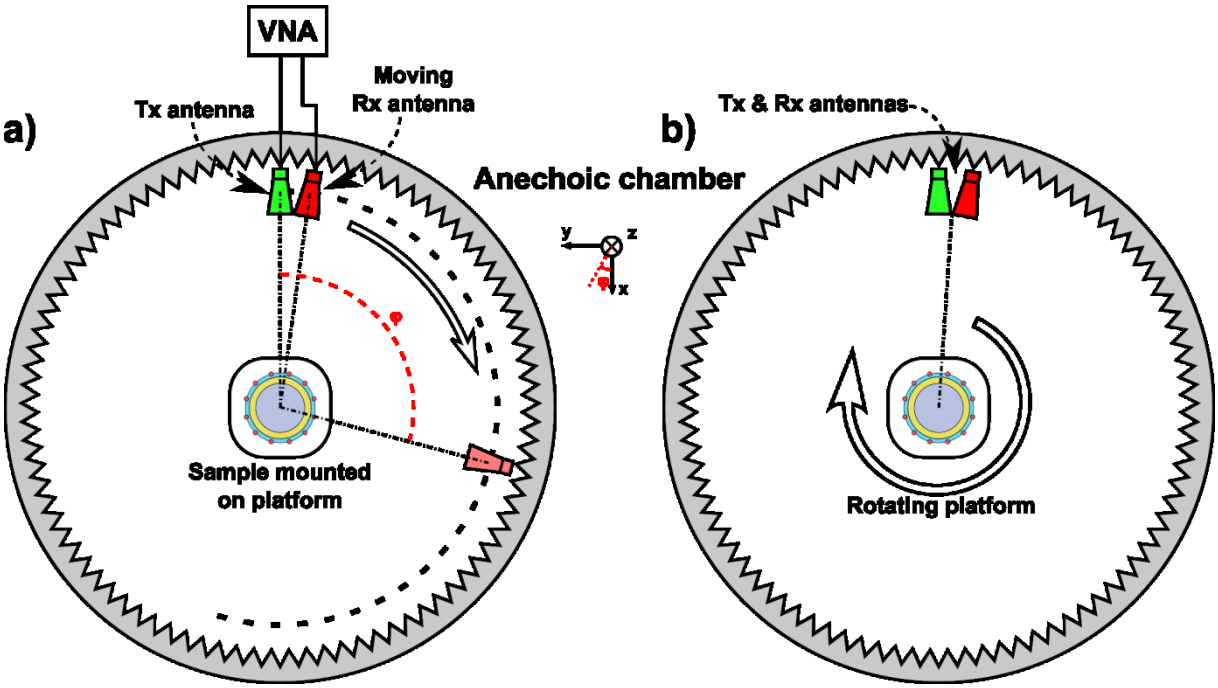

Figure 10. Schematic illustration of the experimental setup used to perform a) bistatic and b) monostatic SCS measurements.

Scattering cross section definition

In HFSS simulations, the bistatic scattering cross section of finite sized objects is calculated as:

$$\sigma_{3D,HFSS}(\varphi) = 4\pi r^2 \frac{|E_{scat}(\varphi)|^2}{|E_{inc}|^2} \quad (8)$$

with E_{scat} being the scattered far field. However, our simulations are performed on a coated cylinder having a height of one unit cell B, and the cylinder is extended to infinity along the z-axis by applying periodic boundary conditions. In order to retrieve the scattering width σ_{2D} of an infinitely long structure from the $\sigma_{3D,HFSS}$ data, the following relation is used:

$$\sigma_{2D}(\varphi) = \sigma_{3D,HFSS}(\varphi)\frac{\lambda}{B^2} \quad (9)$$

An approximate formula relates σ_{2D} to σ_{3D} for a structure with finite height:

$$\sigma_{3D}(\varphi) = \frac{2h^2}{\lambda}\sigma_{2D}(\varphi) \quad (10)$$

where h is the height of the cylinder. Eq 10 therefore allows comparing the simulated data to the experimental one. For a better representation of σ_{3D} in m^2, the following conversion in dB is performed:

$$\sigma_{3D}[\mathrm{dBm}^2] = 10\log_{10}\left(\frac{\sigma_{3D}[\mathrm{m}^2]}{1\mathrm{m}^2}\right) \quad (11)$$

When the receiving antenna is located at the same position as the transmitting one (monostatic configuration), the most widely used term radar cross section is used, it corresponds to the configuration of backscattering.

Finally, the total scattering cross section is defined as:

$$\sigma_{3D\,tot} = \frac{1}{2\pi}\int_0^{2\pi}\sigma_{3D}(\varphi)d\varphi \quad (12)$$

ACKNOWLEDGEMENTS

The authors wish to thank A. Cheraly and D. Bernard for performing the experimental measurements at ONERA Palaiseau.

AUTHOR INFORMATION

Corresponding Authors

Cédric Martel: cedric.martel@onera.fr

Shah Nawaz Burokur: sburokur@parisnanterre.fr

Author Contributions

The manuscript was written through contributions of all authors. All authors have given approval to the final version of the manuscript.

REFERENCES

[1] Salisbury, G. W. Absorbent body of electromagnetic waves, *US Patent 2599944A*, 10 June 1952.

[2] Knott, E. F.; Lunden, C. D. The two-sheet capacitive Jaumann absorber. *IEEE Trans. Antennas Propag.* **1995**, *43*, 1339–1343.

[3] Kumutha, N.; Hariharan, K.; Amutha, N.; Manimegalai, B. Review of RF Cloaking Techniques for Antenna Applications. *ACES* **2018**, *33*, No. 6.

[4] Beeharry, T.; Díaz-Rubio, A.; Asadchy, V.; Ouslimani, H. H.; Tretyakov, S. Step-wise homogeneous passive coatings for reduction of electromagnetic scattering from cylindrical metallic bodies. *J. Opt.* **2020**, *22*, No.105601.

[5] Luukkonen, O.; Costa, F.; Simovski, C. R.; Monorchio, A.; Tretyakov, S. A. A thin electromagnetic absorber for wide incidence angles and both polarizations. *IEEE Trans. Antennas Propag.* **2009**, *57*, 3119–3125.

[6] Kazem Zadeh, A.; Karlsson, A. Capacitive circuit method for fast and efficient design of wideband radar absorbers. *IEEE Trans. Antennas Propag.* **2009**, *57*, 2307–2314.

[7] Li, A.; Singh, S.; Sievenpiper, D. Metasurfaces and their applications. *Nanophotonics* **2018**, *7*, 989–1011.

[8] Wu, B.; Wang, G.; Liu, K.; Hu, G.; Xu, H.-X. Equivalent-circuit-intervened deep learning metasurface. *Mater Des*. **2022**, *218*, No. 110725.

[9] Germain, D.; Seetharamdoo, D.; Burokur, S. N.; de Lustrac, A. Phase-compensated metasurface for a conformal microwave antenna. *Appl. Phys. Lett.* **2013**, *103*, No. 124102.

[10] Wu, K.; Coquet, P.; Wang, Q. J.; Genevet, P. Modelling of free-form conformal metasurfaces. *Nat. Commun.* **2018**, *9*, No. 3494.

[11] Li, H.; Ma, C.; Shen, F.; Xu, K.; Ye, D.; Huangfu, J.; Li, C.; Ran, L.; Denidni, T. A. Wide-angle beam steering based on an active conformal metasurface lens. *IEEE Access* **2019**, *7*, 185264–185272.

[12] Mohammadi Estakhri, N.; Alù, A. Wave-front transformation with gradient metasurfaces. *Phys. Rev. X* **2016**, *6*, No. 041008.

[13] Landy, N. I.; Sajuyigbe, S.; Mock, J. J.; Smith, D. R.; Padilla, W. J. Perfect metamaterial absorber. *Phys. Rev. Lett*. **2008**, *100*, No. 207402.

[14] Sellier, A.; Teperik, T.; Burokur, S. N.; Sabanowski, G.; Piau, G.-P.; de Lustrac, A. Design and model of wideband absorber made of ultrathin metamaterial structures. *Appl. Phys. A* **2014**, *117*, 739-746.

[15] Ra'di, Y.; Simovski, C. R.; Tretyakov, S. A. Thin perfect absorbers for electromagnetic waves: theory, design, and realizations. *Phys. Rev. Appl.* **2015**, *3*, No. 037001.

[16] Jang, Y.; Yoo, M.; Lim, S. Conformal metamaterial absorber for curved surface. *Opt. Express* **2013**, *21*, 24163–24170.

[17] Cheng, Y.; Luo, H.; Chen, F. Broadband metamaterial microwave absorber based on asymmetric sectional resonator structures. *J. Appl. Phys.* **2020**, *127*, No. 214902.

[18] Gu, P. F.; Cao, Z. H.; He, Z.; Ding, D. Z. Design of ultra-wideband RCS reduction metasurface using space mapping and phase cancellation. *IEEE Antennas Wireless Propag. Lett*. **2023**, doi: 10.1109/LAWP.2023.3242659.

[19] Alù, A.; Engheta, N. Achieving transparency with plasmonic and metamaterial coatings. *Phys. Rev. E* **2005**, *72*, No. 016623.

[20] Chen, P.-Y.; Alù, A. Mantle cloaking using thin patterned metasurfaces. *Phys. Rev. B* **2011**, *84*, No. 205110.

[21] Fleury, R.; Monticone, F.; Alù, A. Invisibility and cloaking: Origins, present, and future perspectives. *Phys. Rev. Appl*. **2015**, *4*, No. 037001.

[22] Teperik, T. V.; Burokur, S. N.; de Lustrac, A.; Sabanowski, G.; Piau, G.-P. Experimental validation of an ultra-thin metasurface cloak for hiding a metallic obstacle from an antenna radiation at low frequencies. *Appl. Phys. Lett*. **2017**, *111*, No. 054105.

[23] Asadchy, V. S.; Albooyeh, M.; Tcvetkova, S. N.; Díaz-Rubio, A.; Ra'di, Y.; Tretyakov, S. A. Perfect control of reflection and refraction using spatially dispersive metasurfaces. *Phys. Rev. B* **2016**, *94*, No. 075142.

[24] Ra'di, Y.; Sounas, D. L.; Alù, A. Metagratings: beyond the limits of graded metasurfaces for wave front control. *Phys. Rev. Lett.* **2017**, *119*, No. 067404.

[25] Epstein A.; Rabinovich, O. Unveiling the properties of metagratings via a detailed analytical model for synthesis and analysis," *Phys. Rev. Appl.* **2017**, *8*, No. 054037.

[26] Popov, V.; Boust, F.; Burokur, S. N. Controlling diffraction patterns with metagratings. *Phys. Rev. Appl.* **2018**, *10*, No. 011002.

[27] Zhang, K.; Wang, Y.; Burokur, S. N.; Wu, Q. Generating dual-polarized vortex beam by detour phase: from phase gradient metasurfaces to metagratings. *IEEE Trans. Microw. Theory Tech*. **2022**, *70*, 200-209.

[28] Boust, F.; Lepetit, T.; Burokur, S. N. Metagrating absorber: design and implementation. *Opt. Lett.* **2022**, *47*, 5305–5308.

[29] Tan, Z., Yi, J.; Cheng, Q.; Burokur, S. N. Design of perfect absorber based on metagratings: theory and experiment. *IEEE Trans. Antennas Propag*. **2023**, *71*, 1832–1842.

[30] Popov, V.; Burokur, S. N.; Boust, F. Conformal sparse metasurfaces for wavefront manipulation," *Phys. Rev. Appl.* **2020**, *14*, No. 044007.

[31] Popov, V.; Ratni, B.; Burokur, S. N.; Boust, F. Non-local reconfigurable sparse metasurface: efficient near-field and far-field wavefront manipulations," *Adv. Opt. Mater.* **2021**, *9*, No. 2001316.

[32] Storn, R.; Price, K. Differential evolution – A simple and efficient heuristic for global optimization over continuous spaces. *J. Global Optimization* **1997**, 11, 341–359.

[33] For further details on the differential evolution algorithm, see: scipy.optimize.differential_evolution - SciPy v1.10.0 Manual;

https://docs.scipy.org/doc/scipy/reference/generated/scipy.optimize.differential_evolution.html (accessed: January 2023).

[34] Popov, V.; Yakovleva, M.; Boust, F.; Pelouard, J.-L.; Pardo, F.; Burokur, S. N. Designing metagratings via local periodic approximation: from microwaves to infrared. *Phys. Rev. Appl.* **2019**, *11*, No. 044054.

ToC graphic